Enhanced Electrocatalytic Activity of Low Ni Content Nano Structured NiPd Electrocatalysts Prepared by Electrodeposition Method for Borohydride Oxidation

Mahdieh Zolfaghari, Ali Arab*, and Alireza Asghari

Department of Chemistry, Semnan University, P.O. Box. 35131-19111, Semnan, Iran

ABSTRACT

Some nano structured bimetallic NiPd electrocatalysts were electrodeposited on glassy carbon electrodes using a double potential step chronoamperometry. The morphology of the electrodeposited samples was investigated by field emission-scanning electron microscopy, while their compositions were evaluated using energy dispersive X-ray spectroscopy. It was observed that the electrodeposited samples contained a low Ni content, in the range of 0.80 - 7.10%. The electrodeposited samples were employed as the anode electro-catalysts for the oxidation of sodium borohydride in NaOH solution (1.0 M) using cyclic voltammetry, chronoamperometry, rotating disk electrode, and impedance spectroscopy. The number of exchanged electrons, charge transfer resistances, apparent rate constants, and double layer capacitances were calculated for the oxidation of borohydride on the prepared catalysts. According to the results obtained, the NiPd-2 sample with the lowest Ni content (0.80%), presented the highest catalytic activity for borohydride oxidation compared with the other NiPd samples as well as the pure Pd sample. The anodic peak current density was obtained to be about 1.3 times higher on the NiPd-2 sample compared with that for the Pd sample.

Keywords : Borohydride Oxidation, Electrodeposition, Bimetallic NiPd Electrocatalysts, Nano Structure, Low Ni Content
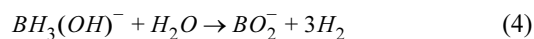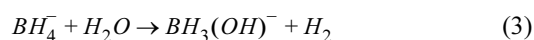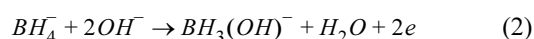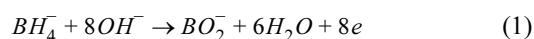
1. Introduction

Direct borohydride fuel cell (DBFC), as one of the best power sources, has been widely considered [1-6] due to some of its unique properties such as high hydrogen content (10.6 wt. %) [7,8], environmental friendliness [9,10], and high open circuit potential as well as high energy density [11].

A complete borohydride oxidation generates 8 electrons, as presented in Eq. (1). However, it is well known that a complete borohydride oxidation is barely found to occur in practice, and an incomplete borohydride oxidation (Eq. 2) and its hydrolysis (Eqs. 3, 4) reduce the efficiency of the fuel cell [12-13]. Therefore, the study and development of the low cost electrocatalysts that can promote a complete oxi-

dation of borohydride is an interesting and important subject.

$$BH_4^- + 8OH^- \rightarrow BO_2^- + 6H_2O + 8e \quad (1)$$

$$BH_4^- + 2OH^- \rightarrow BH_3(OH)^- + H_2O + 2e \quad (2)$$

$$BH_4^- + H_2O \rightarrow BH_3(OH)^- + H_2 \quad (3)$$

$$BH_3(OH)^- + H_2O \rightarrow BO_2^- + 3H_2 \quad (4)$$

Different transition metals including Pt [14-17], Ag [16-19], Au [19-22], Pd [23,24], Os [25], Ni [26,27], Cu [28], and Zn [29] have been considered as the potential electrocatalysts for borohydride oxidation. Palladium, abundantly used as an electrocatalyst for borohydride oxidation, is active for borohydride electro-oxidation as well as its hydrolysis [26,30]. It has been reported that at a low concentration of borohydride, a large anodic current along with a high charge efficiency is obtained on the Pd electrocatalyst [26,30]. In order to reduce the high cost of electrocat-

alysts containing noble metals, bimetallic catalysts have been considered as the potential alternatives. In this regard, the first-row transition metals with unoccupied 3d orbitals (Ni, Cu, Fe, Co, and Zn) have been proposed for a possible enhancement in the electrocatalytic activity for borohydride oxidation [31]. Duan et al. [31] prepared carbon-supported Cu-Pd nanoparticles and used them for borohydride-hydrogen oxidation. They reported that a Cu_1Pd_1/C sample had higher catalytic activity compared to the other prepared catalysts [31]. Martins et al. prepared a series of bimetallic palladium alloys (PdFe, PdAg, PdAu) on the reduced graphene oxide (rGO) and tested them for the oxidation of borohydride [32]. The best performance was observed for the PdAu/rGO sample, with the number of exchanged electrons equal to 5.5 [32]. The Bimetallic Pd-Cu/C catalyst samples with different compositions were tested for the oxidation of borohydride by Behmenyar et al. [33]. Their results revealed that the bimetallic Pd-Cu samples were better electrocatalysts than the pure nano-sized Pd electrocatalyst [33]. Zhiani et al. [34] used a new Ni-Co/C catalyst decorated with Pd particles for borohydride oxidation. They observed that while this catalyst was more reactive than the conventional 10.0 wt.% Pt/C catalyst, its tolerance against poisoning by intermediate products produced during borohydride oxidation was lower [34].

The probable synergistic effects of Ni and Pd compositions create some novel catalytic properties for bimetallic NiPd catalysts that are different from pure Pd and Ni catalysts. The NiPd electrocatalysts have been widely employed for electro-oxidation of alcohols as well as reduction of oxygen [35]. However, studies carried out on the NiPd catalysts for borohydride oxidation are not so much. For example, Hosseini et al. prepared the Ni/NiPd samples by the electrodeposition process followed by the galvanic

replacement technique [36]. They used the prepared samples for the oxidation of borohydride, and their results demonstrated the porous structure of Ni/PdNi coatings with discrete Pd nanoparticles. In addition, the observed anodic peak current density was up to eight times higher on a Ni/PdNi sample than a pure palladium sample [36].

In this work, the low Ni content bimetallic NiPd films were prepared using the double potential step electrodeposition method. The electrodeposited films were characterized by the energy dispersive X-ray (EDX) and field emission-scanning electron microscopy (FE-SEM) analyses. The oxidation of borohydride was investigated by cyclic voltammetry, rotating disk electrode, chronoamperometry, and electrochemical impedance spectroscopy.

2. Experimental

All the reagents used were Merck products and of analytical grade. Ultrapure water was used for the preparation of all aqueous solutions. The glassy carbon rods (diameter = 3 mm) were employed as a substrate for the electrodeposition of the samples. Before each experiment, the surface of the glassy carbon rods was polished with the emery papers of No's 2000, 2500, and 3000 and washed with distilled water, and then the rods were immersed immediately in the electrodeposition bath. The electrodeposition bath contained Na_2SO_4 (0.10 M) and different concentrations of $NiSO_4+PdCl_2$, as presented in Table 1. The bimetallic NiPd samples (labelled as NiPd-1 to NiPd-5) and Pd sample were prepared using two potential steps. The nucleation potential of -0.95 V for 1 s, and growth potential of -0.6 V for 600 s were applied to the electrode. All the electrochemical experiments were done at room temperature in a standard three-electrode cell. A glass frit Ag/AgCl

Table 1. The concentration of Ni and Pd in the electrodeposition bath and in the electrodeposited samples.

Sample	$[Ni^{2+}]/[Pd^{2+}]$ in bath	Atomic ratio of Ni/Pd in sample	%Ni in sample
NiPd-1	10/1	0.042	4.00
NiPd-2	10/2	0.008	0.80
NiPd-3	5/5	0.076	7.10
NiPd-4	2/10	0.019	1.85
NiPd-5	1/10	0.037	3.65
Pd	0/5	-	-

electrode and a platinum plate (1 cm^2) were used as the reference and counter electrodes, respectively. The electrodeposited samples were employed as the working electrodes for the borohydride oxidation in NaOH solution (1.0 M). The cyclic voltammograms, chronoamperograms, and rotating disk electrode experiments were recorded by an Ivium Stat Potentiostat/Galvanostat, model Vertex (Netherland). The electrochemical impedance measurements were performed using an Origaflex Potentiostat/Galvanostat model OGF500 (France) in the frequency range of 100 kHz-20 mHz and an AC amplitude of 10 mV. The EDX, and FE-SEM analyses were carried out by means of a TESCAN FE-SEM microscope, model MIRA3 (Czech).

3. Results and Discussion

3.1. FE-SEM and EDX analyses

Fig. 1 presents the FE-SEM images of the electrodeposited NiPd samples (NiPd-1 to NiPd-5). For comparison, the FE-SEM image of the electrodeposited Pd sample is also depicted in this figure. The structure and morphology of the NiPd samples are different from those for the Pd sample, especially in the case of the NiPd-3 sample where a cauliflower-like structure can be observed. In addition, for the NiPd-1 sample, the polyhedral particles are observed on top of the underlying layer. Another obvious indication in the FE-SEM images of the electrodeposited samples is a distribution of particles with different sizes. The esti-
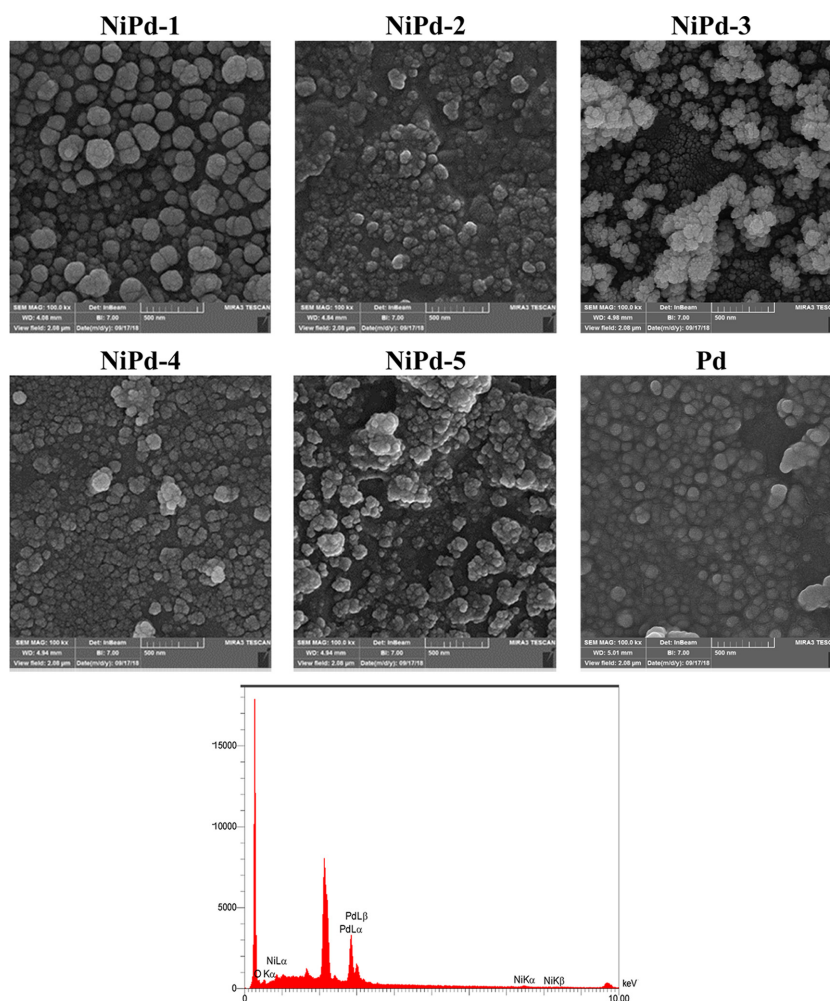

Fig. 1. The FE-SEM images for the electrodeposited samples and the EDX spectrum for the NiPd-1 sample.

NiPd-1   **NiPd-2**   **NiPd-3**
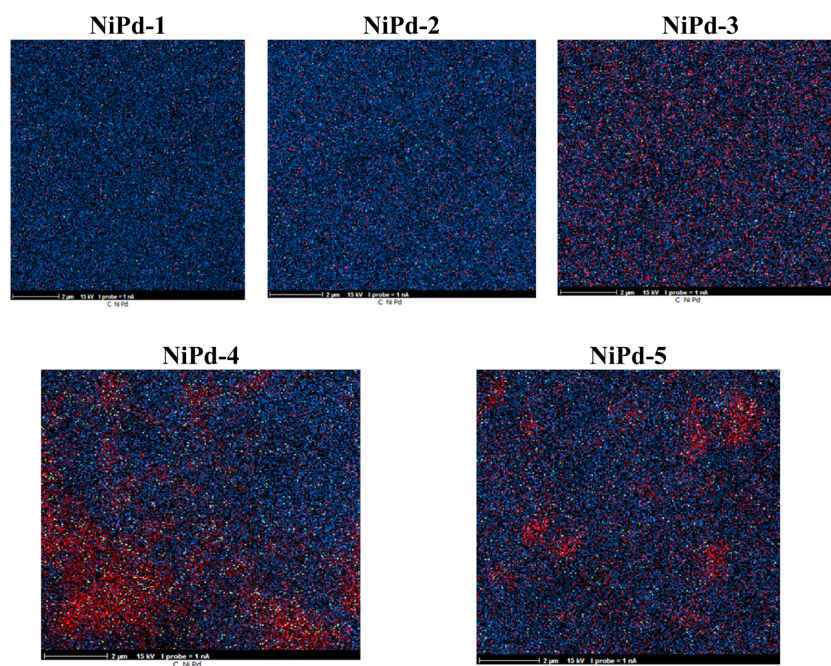
NiPd-4   **NiPd-5**

Fig. 2. The EDAX mapping images of electrodeposited samples. blue: carbon, red: palladium, green: nickel.

mated average size of nano particles is 98, 129, 70, 60, 72, and 56 nm for the Pd, NiPd-1, NiPd-2, NiPd-3, NiPd-4, and NiPd-5 samples respectively.

The EDX spectrum for the NiPd-1 sample is shown in Fig. 1, while for the other electrodeposited samples the EDX spectra are presented in Fig. S1 in the supplementary data. The EDX analyses demonstrate the presence of Ni and Pd entities in the samples which confirm the formation of bimetallic catalysts during the co-deposition process. The composition of the electrodeposited NiPd samples determined by the EDX analysis is collected in Table 1. It can be seen that all the electrodeposited samples contain a low amount of Ni. The lowest (0.80%) and highest (7.10%) Ni contents are related to the NiPd-2 and NiPd-3 samples, respectively. Fig. 2 presents the EDAX mapping images of electrodeposited samples. For NiPd-1, NiPd-2 and NiPd-3 samples a uniform distribution of Ni and Pd particles are observed on the surface of electrode. For NiPd-4 and NiPd-5 samples more accumulation of particles in some areas is obvious.

3.2. Cyclic voltammetry experiments

The cyclic voltammetry experiments were carried out in order to investigate the electrochemical behavior of the electrodeposited samples in NaOH solution (1.0 M). Some of the recorded cyclic voltammograms (CVs) are presented in Fig. 3 (a, b). Assignment of the observed peaks in the CVs for the NiPd samples was carried out using the CVs for the electrodeposited pure Ni and Pd samples as the reference curves (Fig. 3a). The CV for the pure Pd sample represents the reduction peak of palladium hydroxide at around -0.4 V according to the following reaction [37]:

$$Pd(OH)_2 + 2e \rightarrow Pd + 2OH^- \qquad (5)$$

The observed peak at the end of the cathodic half cycle is probably due to the hydrogen adsorption/absorption/evolution. It has been reported that three processes including hydrogen adsorption, absorption, and evolution are not separated from each other on the Pd electrode [38].

In the CV for pure Ni sample, an extended double-layer charging region (-1.0-0.15 V) along with a pair of redox peaks (0.15-0.60 V) were observed. The redox pair is related to the inter-conversion of the Ni(OH)$_2$ and NiOOH entities, as expressed by the
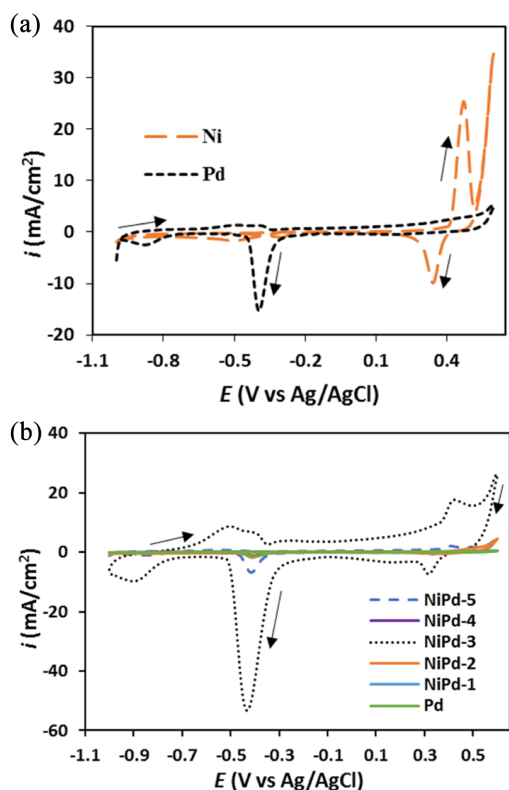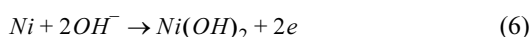
Fig. 3. Cyclic voltammograms for electrodeposited samples for (a) pure Pd and Ni samples and (b) bimetallic Ni-Pd samples and pure Pd in NaOH solution (1.0 M). The potential scan rate is 100 mV s^{-1}.

following equations [39]:

$$Ni + 2OH^- \rightarrow Ni(OH)_2 + 2e \qquad (6)$$

$$Ni(OH)_2 + OH^- \leftrightarrow NiOOH + H_2O + e \qquad (7)$$

In the CVs for the NiPd samples (Fig. 3b), some voltammetric characteristics of pure Ni and Pd samples exist but some new voltammetric characteristics that are quite different from those for pure Ni and Pd electrodes are also observed. This result confirmed that the electrodeposited NiPd samples were not a simple mixture of the Ni and Pd elements. The new electrochemical properties observed for NiPd samples are probably related to the synergistic effects of the Ni and Pd compositions.

Fig. 4 presents the CVs recorded for the electrodeposited Pd and NiPd samples in NaOH solution (1.00

M) containing NaBH$_4$ (0.03 M) at a potential scan rate of 100 mV s^{-1} in the potential range of -1.0-0.6 V. For a better comparison, the CVs for the samples in the absence of borohydride (dashed line) were also overlaid. It is clear in this figure that all the electrodeposited samples exhibit a similar pattern for the borohydride oxidation. For all samples, two anodic peaks (a$_1$, a$_2$) are observed in the forward scan. The first anodic peak (a$_1$) is probably related to the oxidation of H$_2$ and BH$_3$(OH), both produced from the borohydride hydrolysis (Eqs. 3, 4). For the Pd sample, the a$_1$ peak appears at around -0.3 V, while for the NiPd samples, this peak appears at around -0.6 V. Martins et al. [40] have also observed this peak at -0.42 V vs. Ag/AgCl on the Pt electrode in NaOH solution (3.0 M). The second anodic peak (a$_2$) appearing at around -0.2 V can be attributed to the direct oxidation of BH$_4^-$ (Eqs. 1, 2) as reported previously by Gyenge [41], Martins [40], and Benhmenyar [33] on the Pt, Pt and Pd-Cu electrodes respectively.

In the backward scan, the observed peak (c$_1$) at around -0.30 V vs. Ag/AgCl can be attributed to the oxidation of the adsorbed intermediates produced from hydrolysis as well as incomplete oxidation of borohydride. Similar results have also been reported by Gyenge [41] and Concha [42] for the borohydride oxidation on the Pt electrode in alkaline solutions.

According to Fig. 4, the current density value for the a$_2$ peak on the electrodeposited Pd is 28.30 mA cm^{-2}, and for the electrodeposited NiPd samples including NiPd-1, NiPd-2, NiPd-3, NiPd-4, and NiPd-5, it is 33.90, 35.38, 20.54, 16.09, and 30.50 mA cm^{-2}, respectively. Therefore, the NiPd-1, NiPd-2, and NiPd-5 samples have higher catalytic activity than Pd sample for a direct electro-oxidation of borohydride. It seems that the presence of a low amount of Ni in NiPd samples increases reactivity for the borohydride oxidation. Enhancement of reactivity can be attributed to the probable formation of NiPd alloy and variation in the electronic and geometric structures of Pd caused by the incorporation of Ni. As can be seen in EDAX mapping images, better (uniform) distribution of Ni particles on the surface of the electrode is another important factor that affects the catalytic activity of samples.

The ratio of forward to backward peak current densities (a$_2$/c$_1$) was calculated in order to evaluate the catalytic tolerance against the poisoning effects of the adsorbed intermediates generated during hydrolysis
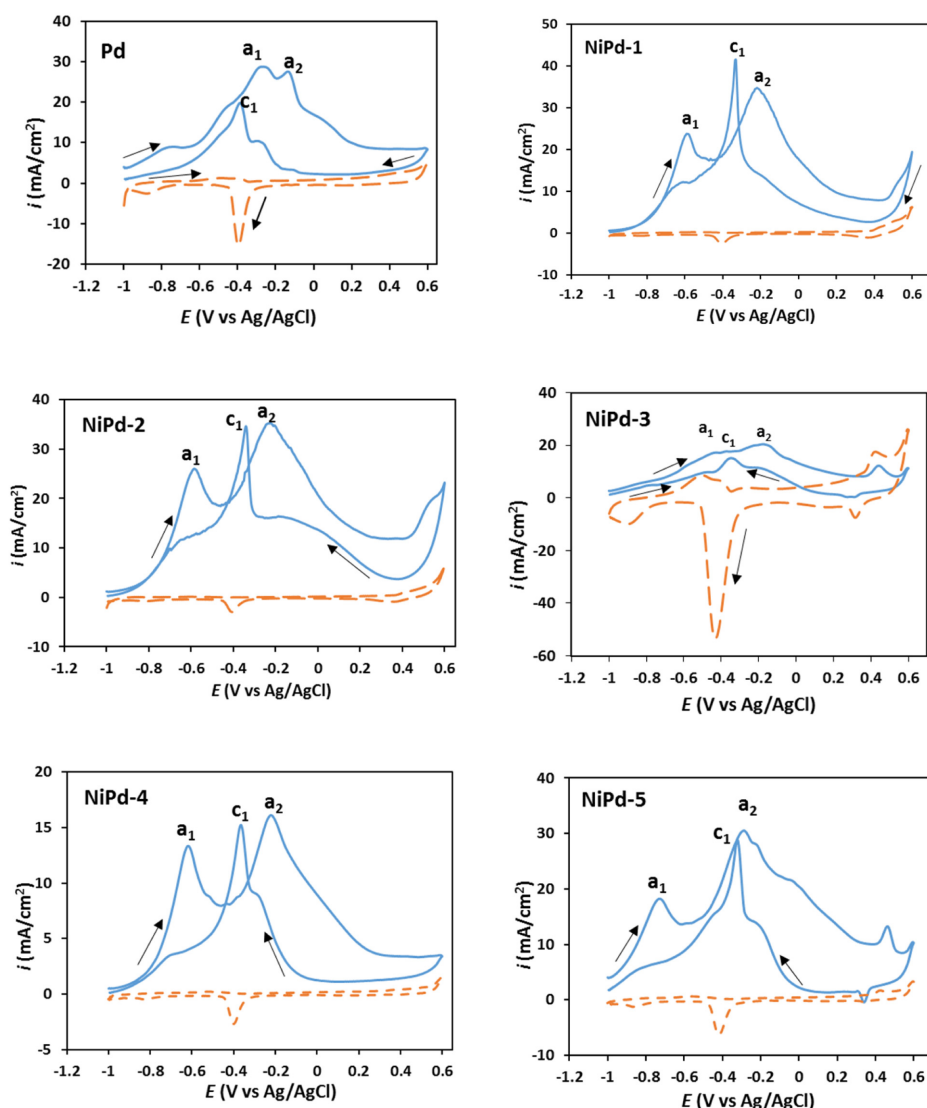
Fig. 4. Cyclic voltammograms for electrodeposited Pd and NiPd samples recorded in NaOH solution (1.0 M) in the absence (dashed lines) and presence (solid lines) of $NaBH_4$ (0.03 M). The potential scan rate is 100 mV s^{-1}.

as well as incomplete oxidation of borohydride. This ratio is 1.35, 0.83, 1.02, 1.11, 1.05, and 1.06 for the Pd, NiPd-1, NiPd-2, NiPd-3, NiPd-4, and NiPd-5 samples respectively. A higher a_2/c_1 ratio indicates that the electrocatalyst oxidizes borohydride more effectively and generate less poisoning intermediates. The smaller value of a2/c1 for NiPd-2 sample compared to the Pd sample can be attributed to the more hydrolysis of borohydride on NiPd-2 sample.

The concentration effect of $NaBH_4$ on the CVs of the electrodeposited samples was also investigated. The CV obtained for the NiPd-1 sample is shown in Fig. S2 in the supplementary data. The anodic current density increased with enhancing the concentration of $NaBH_4$ from 0.02 M to 0.05 M. More enhancing in the concentration of $NaBH_4$ did not change the current density because of the saturation of surface active sites. The inset of Fig. S2 confirms that the anodic peak current density is linearly proportional to the concentration of $NaBH_4$. Similar results can also
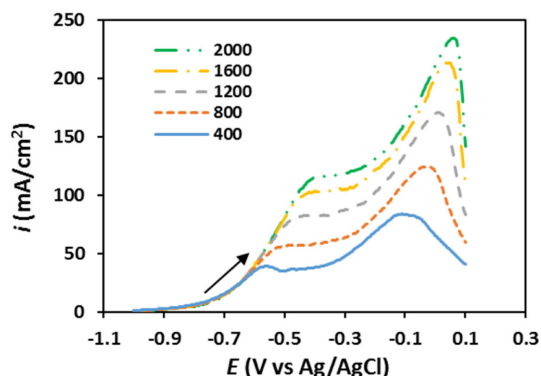
Fig. 5. Linear sweep voltammograms recorded using RDE for NiPd-1 sample in NaOH solution (1.0 M) containing NaBH$_4$ (0.03 M) at different rotation rates. The potential scan rate is 5 mV s^{-1}.

3.3. Rotating disk electrode experiments

The borohydride oxidation on the electrodeposited samples was also evaluated by linear sweep voltammetry (LSV) employing the rotating disk electrode (RDE) technique. The results obtained for the NiPd-1 sample in solution (1.0 M) containing NaBH$_4$ (0.03 M) at the potential scan rate of 5 mV/s are presented in Fig. 5. For other samples, the RDE experiments are reported in Figs. S8-S12 in the supplementary data. It is clear in Fig. 5 that at potentials lower than -0.6 V, the kinetics of charge transfer control the current density and mass transport has no effect on the current density. Therefore, at this potential region, the disk current density is completely independent of the rotation rate [43,44]. A comparison between the RDEs of different samples demonstrates that the current densities obtained for the NiPd-2 sample in the whole studied potential region are higher compared with the other samples in accordance with the CV results.

The kinetic parameters for borohydride oxidation at the investigated electrocatalysts can be estimated using the RDE experiments obtained at different rotation rates. The Koutecky-Levich equation, Eq. (8), which denotes the relationship between the overall current density (*i*) and the kinetic (*i*$_k$) and diffusion-limited (*i*$_d$) current densities is used in order to calculate the number of exchanged electrons (*n*) [45].
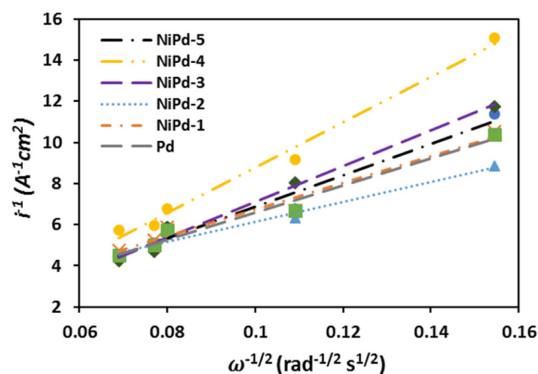

Fig. 6. Koutecky-Levich plots obtained for borohydride oxidation on the electrodeposited samples at the potential of- 0.10 V.

Table 2. The total number of exchanged electrons (*n*) and the apparent rate constants (*k*) obtained for the oxidation of NaBH$_4$ (0.03 M) on the electrodeposited samples. *n*[a] and *n*[b] were calculated using RDE and chronoamperometry measurements respectively.

sample	NiPd-1	NiPd-2	NiPd-3	NiPd-4	NiPd-5	Pd
n[a]	5.99	7.90	4.41	3.48	5.04	4.61
k (cm s^{-1})	0.016	0.056	0.120	0.220	0.053	0.006
n[b]	4.53	7.28	4.06	2.31	4.39	4.22

$$\frac{1}{i} = \frac{1}{i_d} + \frac{1}{i_k} = \frac{1.613\, v^{\frac{1}{6}}}{nFC_b D^{\frac{2}{3}} \omega^{\frac{1}{2}}} + \frac{1}{nFkC_b} \quad (8)$$

where C_b is the borohydride concentration in the solution (mol cm^{-3}), F is the faraday constant (96485 C mol^{-1}), D is the diffusion coefficient of borohydride (1.7×10^{-5} cm^2 s^{-1}) [46-48], v is the kinematic viscosity of the solution (1.14×10^{-2} cm^2 s^{-1}), ω is the angular rotation rate of the electrode (rad s^{-1}), and k is the apparent rate constant (cm s^{-1}).

Considering Eq. (8), the plot of i^{-1} versus $\omega^{-\frac{1}{2}}$ should be linear and the values for *n* and *k* can be calculated using the slope and intercept of this plot. The Koutecky-Levich plots obtained for all the electrodeposited samples in NaOH solution (1.0 M) containing NaBH$_4$ (0.03 M) are presented in Fig. 6 and the calculated values for n and *k* are collected in Table 2.

The values for *n* for the NiPd-1, NiPd-2, and NiPd-5 samples are higher compared to the Pd sample, indicating a more reactivity of these electrodeposited bimetallic catalysts. Furthermore, for the NiPd-2

sample, the value for *n* is close to 8 (7.90), which confirms that the borohydride oxidation occurs almost completely on the NiPd-2 sample.

3.4. Chronoamperometry experiments

Fig. 7 shows the chronoamperograms for different electrocatalysts obtained at their corresponding peak potentials in NaOH solution (1.0 M) containing $NaBH_4$ (0.03 M). A decrease in the current was found, and after approximately 50 s, the steady state current was observable in the chronoamperograms. The steady state current values for the NiPd-1, NiPd-2, and NiPd-5 samples are clearly higher than Pd sample indicating more reactivity of mentioned samples. The results obtained for the chronoamperometry (CA) measurements are in accord with the results of the CV and RDE experiments.

Based on the chronoamperometry measurements, the total number of exchanged electrons (*n*) for borohydride oxidation can also be estimated using the Cottrell equation, Eq. (9), [49].

$$i = nFA\pi^{\frac{1}{2}}D^{\frac{1}{2}}C_b t^{\frac{1}{2}} \tag{9}$$

where *t* is time, and *A* is the surface area of the electrocatalyst (cm^2). The calculated values of *n* for all samples are listed in Table 2. In this Table, one can see that the values of *n* calculated by the two methods are comparable. In addition, the values for *n* for the NiPd-1, NiPd-2, and NiPd-5 samples are larger compared with those in the Pd sample and the maximum value of *n* is related to the NiPd-2 sample in accord with the RDE experiments.
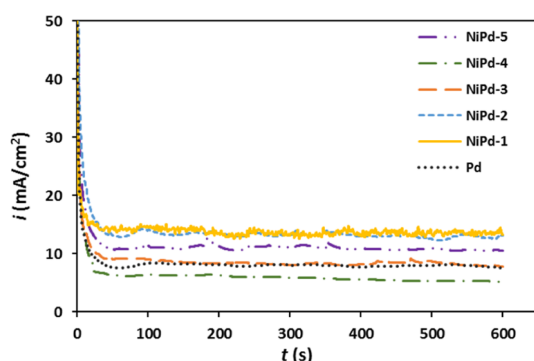

Fig. 7. Chronoamperograms of different samples obtained at their corresponding peak potentials in NaOH solution (1.0 M) containing $NaBH_4$ (0.03 M).

3.5. Electrochemical Impedance Spectroscopy

The Electrochemical Impedance Spectroscopy (EIS) can be used in order to better understand the oxidation of borohydride on the electrodeposited samples. The DC potential was selected at the peak potential (a_2 in Fig. 4) of each sample for the EIS measurements. Fig. 8 presents the Nyquist diagrams obtained for the oxidation of borohydride on the electrodeposited samples in NaOH solution (1.0 M) and in the presence of $NaBH_4$ (0.03 M). All samples represent a similar impedance pattern (a squashed semicircle) for borohydride oxidation. The existence of one semicircle was also confirmed by the Bode and Bode phase plots. For the oxidation of borohydride on the Ni electrodes [50,51], on glassy carbon and Au electrodes [52], similar Nyquist diagrams with one semicircle have also been reported previously. The diameter of the semicircle is directly related to the charge transfer resistance (R_{ct}) of borohydride oxidation. Fig. 8 (inset) presents an equivalent circuit that is compatible with the experimental Nyquist diagrams while the calculated parameters are summarized in Table 3. In an equivalent circuit, R_s denotes the resistance of the solution. Constant phase element (*CPE*) includes the character of the double layer and its impedance is defined by Eq. 10.

$$Z_{CPE}(\omega) = [T(j\omega)^n]^{-1} \tag{10}$$

where ω is the angular frequency of the AC signal, *j* is $\sqrt{-1}$, *n* represents the roughness of the electrode with the values in the 0-1 range. The values for 1, 0, and 0.5 are related to a pure capacitor, resistance, and Warburg behavior, respectively [53]. *T* is related to the double layer capacitance as defined by the $C_{dl} = T^{1/n}R_{ct}^{(1-n)/n}$ equation.

As it could be seen in Table 3, the values for charge transfer resistance (R_{ct}) for the NiPd-2, NiPd-5, and NiPd-1 samples are remarkably smaller compared with the NiPd-3, NiPd-4, and Pd samples. This result obtained certifies that the enhanced electrocatalytic activity is related to the acceleration of electron transfer. Therefore, oxidation of borohydride is faster on the NiPd-2, NiPd-5, and NiPd-1 samples which is in good agreement with the CV, RDE, and CA results. According to these findings, the NiPd-2, NiPd-5, and NiPd-1 samples seem to be a potential anodic electrocatalyst for direct borohydride fuel cells.
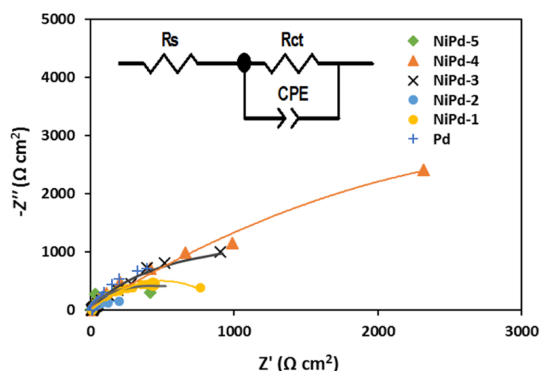
Fig. 8. Nyquist diagrams obtained for oxidation of borohydride on the electrodeposited samples in NaOH solution (1.0 M) containing NaBH$_4$ (0.03 M). Points: experimental data, lines: fitted data. Inset: the equivalent circuit compatible with the experimental Nyquist diagrams.

Table 3. The equivalent circuit parameters obtained for borohydride oxidation on the electrodeposited samples in NaOH solution (1.0 M) containing NaBH$_4$ (0.03 M).

sample	R_s/Ω	R_{ct}/Ω	n	T/Ω^{-1} s^n	$C_{dl}/\mu F$
NiPd-1	13.05	865.6	0.98	0.000057	180
NiPd-2	11.01	419.7	0.86	0.000197	131
NiPd-3	10.52	2770	0.83	0.000265	248
NiPd-4	11.19	5779	0.92	0.000044	39
NiPd-5	10.88	651.7	0.97	0.000062	57
Pd	12.26	2685	0.90	0.000144	130

4. Conclusions

In this work, the bimetallic NiPd electrocatalysts were prepared by electrodeposition through double potential step chronoamperometry. The surface morphology and composition of electrodeposited samples were evaluated by the FE-SEM and EDX analyses respectively. The EDX results demonstrated the low Ni content (0.80 to 7.10 atomic percentage) of the electrodeposited NiPd samples. The SEM results showed that the morphology of the NiPd samples was different from that for the Pd sample and that the Pd nanoparticles in NiPd catalysts were highly dispersed. For NiPd-3 sample with the highest Ni content (7.10%), a cauliflower-like structure was obtained. The electro oxidation of NaBH$_4$ in NaOH solution (1.0 M) was then studied on these samples by the CV, CA, RDE, and EIS techniques.

The number of exchanged electrons, the charge transfer resistances, apparent rate constants, and double layer capacitances were calculated for the oxidation of borohydride on the prepared catalysts. It was observed that the NiPd-1, NiPd-2, and NiPd-5 samples were more reactive than the Pd sample for oxidation of borohydride. It seems that the presence of a low amount of Ni in the bimetallic NiPd catalysts increases the reactivity for borohydride oxidation. Enhancement of the reactivity can be attributed to the probable formation of the NiPd alloys and variation in the electronic and geometric structures of Pd caused by the incorporation of Ni. In addition, the NiPd-2 sample with the lowest Ni content (0.80%) presented the highest catalytic activity toward borohydride oxidation. Therefore, the NiPd samples can be promising anode electrocatalysts for the direct borohydride fuel cell.

Acknowledgment

Supporting Information Paragraph

The Supporting Information contains several main parts including EDX spectra of the electrodeposited Ni-Pd samples, the effect of NaBH$_4$ concentrations on the cyclic voltammograms of Ni-Pd samples, and rotating disk electrode results for Ni-Pd samples.

Supporting Information is available at https://doi.org/10.33961/jecst.2019.00458

References

[1] C. PoncedeLeon, F.C. Walsh, A. Rose, J.B. Lakeman, D.J. Browning, R.W. Reeve, *J. Power Sources*., **2007**, *164(2)*, 441-448.

[2] M.H. Atwan, C.L.B. Macdonald, D.O. Northwood, E.L. Gyenge, *J. Power Sources*., **2006**, *158(1)*, 36-44.

[3] Z.P. Li, B.H. Liu, K Arai., K. Asaba, S. Suda, *J. Power Sources*., **2004**, *126(1-2)*, 28-33.

[4] H. Cheng, K. Scott, *J. Power Sources*., **2006**, *160(1)*, 407-412.

[5] B.H. Liu, S. Suda, *J. Power Sources*., **2007**, *164(1)*, 100-104.

[6] D.M.F. Santos, C.A.C. Sequeira, *Renew. Sust. Energ. Rev*., **2011,** *15(8)*, 3980-4001.

[7] L.B. Wang, C.A. Ma,. X.B. Mao, J.F. Sheng, F.Z. Bai, F.

Tang, *Electrochem. Commun.*, **2005,** *7(12),* 1477-1481.

[8] J. Ma, N.A. Choudhury, Y. Sahai, *Renew. Sust. Enery. Rev.*, **2010**, *14*, 183-199.

[9] I. Merino-Jimenez, M.J. Janik, C. Ponce de Leon, F.C Walsh, *J. Power Sources.*, **2014**, *269*, 498-508.

[10] D.X. Cao, D.D. Chen, J. Lan, G.L. Wang, *J. Power Sources.*, **2009**, *190(2)*, 346-350.

[11] J. Liu, H. Wang, C. Wu, Q. Zhao, X. Wang, L. Yi, *Int. J. Hydrogen Energ.*, **2014**, *39*, 6729-6736.

[12] D. Zhang, G. Wang, Y. Yuan, Y. Li, S. Jiang, Y. Wang, K. Ye, D. Cao, P. Yan, K. Cheng, *Int. J. Hydrogen Energ.*, **2016**, *41(27),* 11593-11598.

[13] D. Zhang, G. Wang, K. Cheng, J. Huang, P. Yan, D. Cao, *J. Power Sources.*, **2014**, *245*, 482-486.

[14] E. Gyenge, *Electrochim. Acta.*, **2004**, *49(6),* 965-978.

[15] J.H. Kim, H.S. Kim, Y.M. Kang, M.S. Song, S. Rajendran, S.C. Han, D.H. Jung, J.Y. Lee, *J. Electrochem. Soc.*, **2004**, *151(7),* A1039-1043.

[16] B. Molina Concha, M. Chatenet, *Electrochim. Acta,* **2009**, *54*, 6119-6129.

[17] B. Molina Concha, M. Chatenet, *Electrochim. Acta.*, **2009**, *54*, 6130-6139.

[18] E. Sanli, H. Celikkan, B. Zuhtu Uysal, M.L. Aksu, *Int .J. Hydrogen Energ.*, **2006**, *31(13)*, 1920-1924.

[19] M. Chatenet, F. Micoud, I. Roche, E. Chainet, *Electrochim. Acta.*, **2006,** *51*, 5459-5467.

[20] S.C. Amendola, P. Onnerud, M.T. Kelly, P.J. Petillo, S.L. Sharp-Goldman, M. Binder, *J. Power Sources.*, **1999**, *84(1),* 130-133.

[21] H. Cheng, K. Scott,. *Electrochim. Acta.*, **2006**, *51(17),* 3429-3433.

[22] D.X. Cao, Y.Y Gao, G.L. Wang, R.R. Miao, Y. Liu, *Int. J. Hydrogen Energ.*, **2010**, *35(2),* 807-813.

[23] C. Cenk, F.G. Boyaci San, H.I. Sarac, *J. Power Sources.*, **2008**, *185(1),* 197-201.

[24] J.Q. Yang, B.H. Liu, S. Wu, *J. Power Sources.*, **2009**, *194(2),* 824-829.

[25] M.H. Atwan, D.O. Northwood, E.L. Gyenge, *Int. J. Hydrogen Energ.*, **2005**, *30(12)*, 1323-1331.

[26] B.H. Liu, Z.P. Li, S. Suda, *J. Electrochem. Soc.*, **2003**, *150(3),* A398-402.

[27] K.L. Wang, J.T. Lu, L. Zhuang, *J. Phys. Chem. C.*, **2007**, *111(20),* 7456-7462.

[28] D.H. Duan, S.B. Liu, Y.P. Sun, *J. Power Sources.*, **2012**, *210*, 198-203.

[29] D.M.F. Santos, C.A.C. , *J. Electrochem. Soc.*, **2010**, *157(1),* B13-B19.

[30] B.H. Liu, Z.P. Li, S. Suda, *Electrochim. Acta.*, **2004**, *49(19),* 3097-3105.

[31] D.H Duan, X. You, J. Liang, S. Liu, Y. Wang, *Electrochim. Acta.*, **2015,** *176*, 1126-1135.

[32] M. Martins, B. Sljukic, O. Metin, M. Sevin, C.A.C. Sequera, T. Sener, D M.F. Santos, *J. Alloys Compd.*, **2017**, *718*, 204-214.

[33] G. Behmenyar, A.N. Akın, *J. Power Sources.*, **2014**, *249*, 239-246.

[34] M. Zhiani, I. Mohammadi, *Fuel*, **2016**, *166*, 517-525.

[35] R Awasthi, RN. Anindita, Singh, *Open Catal. J.*, **2010**, *3(1),* 70-78.

[36] MG. Hosseini, M. Abdolmaleki, *Int. J. Hydrogen Energ.*, **2013**, *38(13)*, 5449-5456.

[37] J. Bagchi, S.K. Bhattacharya, *Transit. Metal. Chem.*, **2008**, *33(1),* 113-120.

[38] J.T. Zhang, M.H. Huang, H.Y. Ma, F. Tian, W. Pan, S.H. Chen, *Electrochem. Commun.*, **2007**, *9(6),* 1298-1304.

[39] M.A. Abdel Rahim, H.B. Hassan, R.M. Abdel Hamid, *J. Power Sources.*, **2006**, *154(1),* 59-65.

[40] J.I. Martins, M.C. Nunes, R. Koch, L. Martins, M. Bazzaoui, *Electrochim. Acta.*, **2007**, *52(23),* 6443-6449.

[41] E. Gyenge, *Electrochim. Acta.*, **2004**, *49(6),* 965-978.

[42] B. Molina Concha, B. M. Chatenet, *Electrochim. Acta.*, **2009,** *54(26),* 6119-6129.

[43] Southampton Electrochemistry Group. Instrumental Methods in Electrochemistry. Chichester: Ellis Horwood Limited, **1985**.

[44] A.Tegoua, S.Papadimitrioua, I.Mintsoulia, S.Armyanovb, E. Valovab, G. Kokkinidisa, S. Sotiropoulosa, *Catal. Today.*, **2011**, *170*, 126-133.

[45] J. Koutecky, J.V.G. Levich, *Zh. Fiz. Khim.*, **1958**, *32(7),* 1565-1575.

[46] M. Simoes, S. Baranton, C. Cou tanceau, *J. Phys. Chem. C.*, **2009**, *113(30),* 13369-13376.

[47] M. Chatenet, F. Micoud, I. Roche, E. Chainet, *Electrochim. Acta.*, **2006**, *51*, 5459-5467.

[48] M. Simoes, S. Baranton, C. Coutanceau, *Electrochim. Acta.*, **2010**, *56(1),* 580-591.

[49] J..L Wei, X.Y. Wang, Y. Wang, Q.Q. Chen, F. Pei, Y.S. Wang, *Int. J. Hydrogen Energ.*, **2009**, *34*, 3360-3366.

[50] MG. Hosseini, M. Abdolmaleki, S. Ashrafpoor, *Chin. J. Catal.*, **2012**, *33(11-22),* 1817-1824.

[51] MG. Hosseini, R. Mahmoodi, *J. Colloid Interf. Sci.*, **2017**, *500*, 264-275.

[52] R. Valiollahi, R. Ojani, JB. Raoof, *Electrochim. Acta.*, **2016**, *191*, 230-236.

[53] F. Gobal, M. Faraji, *Electrochim. Acta.*, **2013**, *100*, 133-139.